

# Nucleonic resonance effects in the $\pi$ meson photoproduction

Qiang Zhao<sup>a</sup>, J.-P. Didelez<sup>a</sup>, M. Guidal<sup>a</sup>, B. Saghai<sup>b</sup>

<sup>a</sup>Institut de Physique Nucléaire, F-91406 Orsay Cedex, France

<sup>b</sup>Service de Physique Nucléaire, DAPNIA-DSM, CEA/Saclay,  
F-91191 Gif-sur-Yvette, France

---

## Abstract

The process  $\pi^+ \pi^-$  close to threshold is investigated focusing on the role played by the s- and u-channel nucleonic resonances. For this purpose, a recent quark model approach, based on the SU(6)  $\times$  O(3) symmetry with an effective Lagrangian, is extended to the  $\pi$  meson photoproduction. Another non-diagrammatic process, the t-channel  $\pi^0$  exchange, is also included. The diagrammatic contribution is produced by the t-channel Pomeron exchange. Contributions from non-diagrammatic s- and u-channel process are found small in the case of cross sections and polarization observables at forward angles. However, backward angle polarization asymmetries show high sensitivity to this non-diagrammatic process. Different prescriptions to keep gauge invariance for the Pomeron exchange amplitudes are investigated. Deviations from the exact SU(6)  $\times$  O(3) symmetry, due to the configuration mixing, are also investigated.

---

**PACS:** 12.39.-x, 25.20.Lj, 13.60.Le, 13.88

**Keywords:** Phenomenological quark model, Photoproduction reactions, Meson production, Polarization

## 1 Introduction

A well established feature in vector meson photoproduction at low momentum transfer and high energies is that the diffractive scattering governs the reaction mechanism [1]. With the advent of the new high intensity beam facilities, like JLAB, ELSA, GRAAL, SPring-8, the study of this field in both low energy ( $E = 2$  GeV) and/or high momentum transfer ( $|t| \approx 1$  (GeV/c) $^2$ ) becomes possible. In these regimes, deviations from pure diffractive phenomena are expected, which should show up, especially in polarization observables.

In recent works, the diffractive component is dealt with as a  $t$ -channel pomeron exchange [2-5], where the pomeron is treated as a  $C = +1$  isoscalar photon. For the non-diffractive contributions, various sources have been explored. In Ref. [6], the  $t$ -channel pseudoscalar mesons ( $J = 0$ , i.e.  $^0$  and  $^-$ ) exchanges are in general found to produce small contributions at small momentum transfers. Here, it will be interesting to study the nature of the parity exchange at low energy, namely, the interplay between diffractive scattering which is intrinsically a natural parity exchange and the pseudoscalar meson exchange which is an unnatural parity exchange process.

Another exciting topic concerns the possible violation mechanisms of the Okubo-Zweig-Iizuka (OZI) rule [7]. Such a violation has recently been reported in the  $\bar{p}n$  and  $p\bar{p}$  annihilation experiments [8]. Theoretically, these phenomena can not be explained by conventional approaches based on the two-step OZI allowed final state interaction with the intermediate kaon formation. Various models have been proposed to account for this, initiating the search for strangeness components in nucleons via the meson photoproduction near threshold [9-11]. Then, one needs to investigate on the one hand OZI evading processes and on the other hand the role of the strangeness content of the proton via  $s\bar{s}$  knock-out reactions.

Another important component in the reaction mechanism at low energies is expected to be the contributions from  $s$ - and  $u$ -channel resonance excitations. At present time, there is no systematic investigation of the role played by the resonances in the meson photoproduction, which, however, might be another important non-diffractive source contributing near threshold. Although a recent work [12] taking into account the  $s$ - and  $u$ -channel  $NN$  coupling has been carried out, the contributions from resonances have not been included there. In fact, at hadronic level, the unknown  $NN$  couplings have been the barrier to go further to include the resonances since one has to introduce at least one parameter for each  $NN$  coupling vertex, therefore, a large number of parameters will appear in the theory. On this point, the quark model approach shows great advantages: in the exact  $SU(6) \otimes O(3)$  symmetry limit, the quark-vector meson interactions can be described by the effective Lagrangian

with only two parameters. The main purpose of the present work is, therefore, to focus on this aspect using a quark-model based effective Lagrangian approach in line with a recent work [13,14]. Here, we wish to emphasize that in the latter work, a very preliminary study of the resonance contributions to the meson photoproduction was performed and, especially, the dominant di-ractive contribution was not included. Therefore, it was impossible to constrain the parameters there and an approximate estimation was made for only the differential cross section from the resonance contributions. In this work, the dominant di-ractive process has been introduced consistently with the quark model approach, and a search is performed to constraint the parameters. This set of ingredients is expected to make possible a reliable estimation of the small, but significant, contributions from the nucleonic resonances to the reaction mechanism. Our results show that the resonances (with mass  $M_R \approx 2.0$  GeV) play a non-negligible role, especially in polarization observables, in spite of the rather high meson production threshold ( $E^{\text{thres}} \approx 1.57$  GeV corresponding to the total center-of-mass energy  $\sqrt{s} = 1.96$  GeV).

As a first step of study in the energy region near threshold, we employ a non-relativistic quark potential to describe the quark motion. As it has been shown in Ref. [15], the non-relativistic formulation remains a viable approximation due mainly to the effective parameters such as the constituent quark mass. To partly cure the shortcoming arising from the non-relativistic quark potential, a widely used Lorentz boost is introduced in the spatial integrals [16].

For the pure di-ractive process, our formalism embodies a model treating the Pomeron like a  $C = +1$  isoscalar photon [2,5]. It is the extrapolation from the high energy region ( $E = 6.45$  GeV) down to the low energy region. Thus, no free parameters are introduced. The resonance contributions drop quickly with the energy increasing, and almost vanish when the photon energy goes above roughly 2.8 GeV. So, at higher energies, the meson photoproduction cross section is generated by the di-ractive process. Therefore, with such a Pomeron exchange term, this model can be applied to the meson production from threshold up to the higher energy region (i.e.  $E = 10$  GeV) where the s- and u-channel contributions are negligible. Although our interest is to study the energy region near threshold, we emphasize that a reliable estimation of the di-ractive contribution in this energy region must be the prerequisite to further investigations, especially, when focusing on the small non-di-ractive contributions.

The contribution from  $^0$  exchange is also included in this work. However, we find that at  $E = 2.0$  GeV, it is quite negligible in comparison with not only the Pomeron exchange in the small  $\mathbf{q}\mathbf{q}$  region, but also the resonance contributions in the large  $\mathbf{q}\mathbf{q}$  region. We do not include the amplitude for the  $^0$  exchange in this work, since although the meson has larger decay branching ratio for  $^0$  than for  $^1$ , which means that the coupling is stronger than

the  $^0$  coupling, a recent analysis [17] of the photoproduction shows that  $g_{NN}$  is smaller than  $g_{NN}$  by roughly a factor of 7, which leads to negligible effects due to the exchange in the production.

In section 2, we present the effective Lagrangian for the quark-vector-meson coupling and the amplitude for the Pomeron and  $^0$  exchanges. In section 3, the numerical results for the differential cross section and polarization observables are reported. As a test of the model, we present the total cross section up to  $E = 10$  GeV in comparison with the experimental data. We also present comparisons, for the three density matrix elements  $^0_{00}$ ,  $Re ^0_{10}$  and  $^0_{11}$ , between our predictions and the experimental results, showing that the diffractive contribution has been treated in a reliable manner. The predictions for the three density matrix elements are presented at  $E = 20$  GeV. Possible OZI suppression effects are also discussed. In section 4, Pomeron exchange amplitudes, due to different schemes of taking into account the gauge invariance, are investigated. Section 5 is devoted to the study of the  $SU(6) \times O(3)$  symmetry breaking due to the configuration mixing effects. Conclusions are given in section 6.

## 2 Form alism

In Ref. [14], the quark model approach to vector meson photoproduction with an effective Lagrangian in the resonance region has been developed. In the following Subsection we summarize the main points of that approach and extend it to the meson photoproduction process. Notice that in Ref. [14] the latter process was investigated only qualitatively, for the following reasons: i) the di ractive Pomeron exchange, which plays a dominant role in the reaction mechanism, is absent in that work, ii) this latter shortcoming prevents any parameter search, iii) also, the polarization observables can not be investigated within Ref. [14] formalism.

In the remaining two subsections, the di ractive Pomeron exchange and the non-di ractive  $\pi^0$  exchange are presented.

### 2.1 Effective Lagrangian for quark-vector-meson coupling

The formalism used here is based on the  $SU(6) \times O(3)$  symmetry for the 3-quark baryon system. We suppose that the meson is produced from an elementary process described by an effective Lagrangian where the meson is treated as a point-like elementary particle. As we will discuss later, deviations from this symmetry are a valuable source of information about the structure of the intervening hadrons.

The effective Lagrangian introduced for the quark-meson coupling has the following form :

$$L_{\text{eff}} = \bar{q} p + \bar{q} e_q A + \bar{q} (a + \frac{ib}{2m_q} q)_{\text{m}} ; \quad (1)$$

where  $\bar{q}$  and  $\bar{q}$  represent the quark and anti-quark fields, respectively, and  $\text{m}$  denotes the vector meson field. The two parameters,  $a$  and  $b$  represent the vector and tensor couplings of the quark to the vector meson, respectively, and  $m_q = 330 \text{ MeV}$  is the constituent quark mass.

With the above effective Lagrangian, at tree level, the non-di ractive transition amplitudes can be expressed as the sum of the contributions from s-, u-, and t-channel:

$$M_{fi} = M_{fi}^s + M_{fi}^u + M_{fi}^t ; \quad (2)$$

Given that the t-channel contribution,  $M_{fi}^t$ , is proportional to the charge of the final state meson, it does not contribute in the case of neutral meson photoproduction. The transition amplitudes from s- and u-channel can be written as:

$$M_{fi}^{s+u} = i! \sum_j^X h N_f H_m N_j i h N_j j \frac{1}{E_i + !} h_e N_{i!} - h_e N_{i!} \\ + i! \sum_j^X h N_f h_e \frac{1}{E_i - !} N_j i h N_j H_m N_{i!}; \quad (3)$$

with  $H_m = \bar{a} + \frac{ib}{2m_q}$  for the quark-meson coupling vertex, and

$$h_e = \sum_1^X e_l r_l (1 - \hat{k}) e^{ik \cdot \hat{r}}; \hat{k} = \frac{k}{!}; \quad (4)$$

Here,  $l = 1, 2, 3$ , denotes the three quarks of the initial or final state nucleons, and  $e_l$  is the charge of the  $l$ th quark. The matrix,  $= \delta^{ij}$ , where  $\delta^{00}$  and  $\delta^{11}$  are the Dirac matrices. The kinematic variables are,  $k$ : the momentum of the incident photon;  $!$ : the photon energy;  $!$ : the energy of the outgoing meson;  $E_j$ : the energy of the intermediate state in the s- and u-channels;  $E_i$ : the energy of the initial state nucleon. It should be noted that in Eq. (3), we have omitted the contact term derived from the s- and u-channels since it is proportional to the charge of the outgoing meson, therefore, vanishes in the neutral meson production processes.

The explicit expressions for the longitudinal and transverse s- and u-channel transition matrices have been derived in Ref. [14]. The transition amplitudes for each resonance in the s-channel below 2 GeV are included explicitly, while the resonances above 2 GeV with a given quantum number  $n > 2$  in the harmonic oscillator basis of the quark model are treated as degenerate. The contributions from the u-channel resonances are divided into two parts as well. The first part contains the baryons with the quantum number  $n = 0$ , which includes the spin 1/2 states, and the spin 3/2 resonances. Since the mass splitting between the spin 1/2 and spin 3/2 resonances with  $n = 0$  is significant, they have to be treated separately. The second part in the u-channel comes from the excited resonances with quantum number  $n = 1$ . As the contributions from the u-channel resonances are not sensitive to the precise mass positions, they can also be treated as degenerate. In the meson photoproduction, because of the isospin conservation, the meson photoproduction gets contributions only from isospin 1/2 resonances. Therefore, only the nucleon pole term ( $n = 0$ ) and those intermediate excited states ( $n > 0$ ) with isospin 1/2 contribute in this reaction. Also, the Moorhouse selection rule [18] suppresses those states belonging to representation  $(70, \frac{1}{2}; 8)$  from contributing in the photon excitations of the proton target. Therefore, in the NRQM

symmetry limit, there are only 8 intermediate nucleonic resonances appearing in the s-channel with  $n = 2$ . In Table 1, the NRQM wave-functions of these resonances are presented with their masses  $M_R$  and total widths  $\Gamma$ .

The transition amplitudes can then be expressed in terms of the 12 independent helicity amplitudes, which are related to the spin observables and the density matrix elements [19,20].

The general transition amplitude for the s-channel excited states in the helicity space has the following form :

$$H_{av}^J = \frac{2M_R}{s - M_R(M_R - i(\mathbf{q}))} h_{av}^J; \quad (5)$$

where  $\frac{p}{s} = E_i + !_i = E_f + !_m$  is the total energy of the system,  $E_i$  and  $E_f$  are the energies of the nucleons in the initial and final states, respectively,  $h_{av}^J$  are the helicity amplitudes, and  $i(\mathbf{q})$ , which is a function of the final state momentum  $\mathbf{q}$ , denotes the momentum dependence of the total width of the resonance  $\Gamma$  [16].

The differential cross section has the expression :

$$\frac{d\sigma}{dt} = \frac{e(E_f + M_N)(E_i + M_N)}{16s} \frac{1}{2} \sum_{a=1}^3 \sum_{v=0,1}^J H_{av}^J; \quad (6)$$

Table 1

Resonances in the s-channel, with their assignments in the SU(6)  $\otimes$  O(3) symmetry limit, are given in the first and second columns, respectively. The masses ( $M_R$ ) and total widths ( $\Gamma$ ), used in this work, given in columns third and fourth, respectively, are taken from Ref. [21].

Resonances	SU(6)	O(3)	$M_R$ (MeV)	$\Gamma$ (MeV)
$P_{11}(1440)$	$N(^2S_S^0)_{\frac{1}{2}^+}$		1440	350
$D_{13}(1520)$	$N(^2P_M)_{\frac{3}{2}^-}$		1520	120
$S_{11}(1535)$	$N(^2P_M)_{\frac{1}{2}^-}$		1535	150
$F_{15}(1680)$	$N(^2D_S)_{\frac{5}{2}^+}$		1680	130
$P_{11}(1710)$	$N(^2S_M)_{\frac{1}{2}^+}$		1710	100
$P_{13}(1720)$	$N(^2D_S)_{\frac{3}{2}^+}$		1720	150
$P_{13}(1900)$	$N(^2D_M)_{\frac{3}{2}^+}$		1900	400
$F_{15}(2000)$	$N(^2D_M)_{\frac{5}{2}^+}$		2000	450

where  $M_N$  represents the mass of the nucleon, and  $k$  denotes the momentum of the incoming photon in the cm. system.

In the harmonic oscillator basis, the factor  $e^{-\frac{q^2+k^2}{6^2}}$  comes from the integrations over the 3-quark baryon wave-functions, and plays a role like a form factor for the quark-meson and quark-photon vertices [22]. Here,  $\epsilon = 410$  MeV is the commonly used value for the harmonic oscillator strength, and no additional "cut-off" parameter is needed. Thus, only two parameters,  $a$  and  $b$  in Eq. (1) are introduced by the effective Lagrangian for the s- and u-channel non-diffractive production. It should be noted that the gauge invariance of the amplitudes from the effective Lagrangian has been fixed. Moreover, the above factor is implemented with the Lorentz boost, to take into account the relativistic effects.

## 2.2 t-channel diffractive Pomeron exchange

We use the Pomeron exchange model by Donnachie and Landshoff [2] to produce the diffractive contribution in this work. In the model, the Pomeron mediates the long range interaction between a confined quark and a nucleon. Although the nature of the Pomeron exchange is still unclear, it has been shown that the Pomeron exchange based on the Regge phenomenology is one of the most successful approaches to high energy elastic scattering. Also, it has been shown that the Pomeron behaves rather like a  $C = +1$  isoscalar photon.

With the Pomeron-photon analogy picture, the Pomeron-nucleon coupling is described by the vertex:

$$F(t) = \beta_0 f(t); \quad (7)$$

where  $t$  is the Pomeron momentum squared,  $\beta_0$  gives the strength of the coupling of the single Pomeron to a light constituent quark.  $f(t)$  represents the form factor which is taken to be the same as the isoscalar nucleon electromagnetic form factor, therefore it has the following expression:

$$f(t) = F_1(t) = \frac{(4M_N^2 - 2.8t)}{(4M_N^2 - t)(1 - t=0.7)^2}; \quad (8)$$

For the  $P$  vertex, the lowest order diagram for the quark pair creation in Ref. [5] is used for the  $s\bar{s}$  creation, but has been extrapolated to the limit of  $Q^2 = 0$ , namely, the process with real photons. A bare photon vertex is introduced for the quark-photon interaction, which has the same form as the

quark-photon coupling in Eq. (1). Here, we use the "on-shell approximation" for the quark- vertex, i.e.  $V$  in Fig. 1:

$$V(p - \frac{1}{2}q; p + \frac{1}{2}q) = f M ; \quad (9)$$

where  $f$  represents the coupling strength and is fixed by the  $\pi^+ \pi^-$  decay width  $\pi^+ \pi^-$  with the following relation:

$$\pi^+ \pi^- = \frac{8}{3} \frac{e^2 e_Q^2}{M} \left( \frac{f^2}{M} \right) ; \quad (10)$$

where  $e_Q = 1/3$  is the charge factor of the  $s$  quark in terms of the charge of electron.

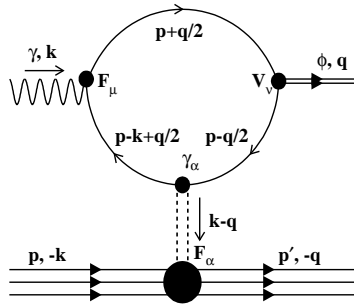


Fig. 1. Pomeron exchange diagram in the  $\pi$  meson photoproduction.

Therefore, the current matrix element can be written as:

$$h_{f\bar{f}}(p_f; q) = \bar{u}(p_f) F_\mu(p_f) \gamma^\mu \bar{u}(p_i) = 2 \bar{u}(p_f) \gamma^\mu (q) G_P(s; t) \bar{u}(p_f) F_\mu(p_f) ; \quad (11)$$

where  $u(p_i)$  and  $\bar{u}(p_f)$  are the initial and final state Dirac spinors of the protons with four-momenta  $p_i$  and  $p_f$ , respectively.  $k$  and  $q$  are the four-momenta of the incoming photon and outgoing meson, respectively.  $\gamma$  is the polarization vector of the produced meson, and the factor 2 counts the equivalent contributions from Pomeron-quark and Pomeron-anti-quark interactions.  $G_P(s; t)$  is related to the Regge trajectory of the Pomeron and has the form:

$$G_P(s; t) = i(\bar{s})^{(t)1} ; \quad (12)$$

where  $t = 1 + \frac{1}{2}t$  is the Regge trajectory of the Pomeron. The form factor  $\frac{2}{0} = (\frac{2}{0} + p^2)$  is introduced for each on-shell quark line with four-momentum  $p$ . In Eq. (11),  $t(k; q)$  represents the loop tensor and it has the following expression for the contributing terms:

$$t(k; q) = (k + q) \cdot g - 2k \cdot g \quad : \quad (13)$$

Note that we have used the free constituent quark propagator  $S(p) = \frac{i}{p + m_s}$  for the strange quark with mass  $m_s$ . However, this latter mass term vanishes due to the odd number of matrices in the trace for the loop. To preserve gauge invariance, we have adopted the transformation given in Ref. [11]. In section 4, we detail this point to investigate the effects from the different Pomeron exchange amplitudes due to the various schemes for fixing the gauge.

The above discussion shows that such a Pomeron exchange picture is consistent with the processes described by the effective Lagrangian in Eq. (1). Qualitatively, we suppose that the effective Lagrangian governs the coupling of the vector meson to the constituents and  $\bar{s}$  in the Pomeron exchange. Then, the tensor part vanishes because odd number of matrices appears in the loop integration. Only the vector part couples to the point-like vector meson effectively with the coupling constant  $a$ . This result reproduces the "on-shell approximation" for the  $s\bar{s}$ -vertex. With this analogy, the parameter  $a$  in the effective Lagrangian can be expressed as:

$$a = f/M \quad : \quad (14)$$

From Eq. (10), we have  $f^2/M = 26.6 \text{ MeV}$ , then the value of parameter  $a = 0.16$  is derived. This value is comparable with what we use for the s- and u-channel quark-meson coupling. However, such an analogy does not imply a rigorous constraint on the parameter  $a$  since generally, the tensor coupling will contribute especially in the large  $|j|$  region in the s- and u-channel. But it provides us with a consistency test between the Pomeron exchange picture and the s- and u-channel non-diffractive description. As discussed in the next section, with the constraint from the differential cross section,  $|j| = 0.15$  and  $p^0 j = 0.3$  give reasonable estimation of the contributions from the effective Lagrangian.

In the case of real photons, that is  $Q^2 = 0$ , the explicit expressions for the Pomeron exchange for the transverse and longitudinal production are

$$H_{av} = 32 \frac{p}{2} e \frac{\frac{2}{0} m f}{\frac{2}{0} F_1(t)} \frac{\frac{2}{0} F_1(t)}{(\frac{2}{0} t)(\frac{2}{0} + M^2 - t)} ({}^0S) \frac{t}{t-1} M_T(P) + M_L(P) l_v ; \quad (15)$$

where

$$\begin{aligned}
M_T(P) = & \frac{h}{(1 + 1)} + \frac{q^2}{E_f + M_N} + \frac{k^2}{E_i + M_N} \\
& + \left( \frac{1}{E_f + M_N} + \frac{1}{E_i + M_N} \right) q \frac{i}{k} \\
& + \left( \frac{1}{E_f + M_N} + \frac{1}{E_i + M_N} \right) i \quad (k - q) \\
& + \frac{2}{E_f + M_N} \quad k - q \\
& \frac{2}{E_f + M_N} i \quad ( - q)k \\
& + \frac{2}{E_i + M_N} i \quad ( - k)k \quad ;
\end{aligned} \tag{16}$$

and

$$\begin{aligned}
M_{\bar{q}q} M_L(P) = & \frac{h}{(1 + 1)} \left( \frac{q^2}{E_f + M_N} + \frac{k^2}{E_i + M_N} \right) \\
& 2 \frac{! \bar{q}q^2}{E_f + M_N} + ! \left( \frac{1}{E_f + M_N} - \frac{1}{E_i + M_N} \right) q \frac{i}{kq} \\
& (! \bar{q}q^2 - ! q \frac{2}{E_i + M_N} i \quad ( - k) \\
& + (! \bar{q}q^2 - ! q \frac{2}{E_f + M_N} i \quad ( - q) \\
& + ! \left( \frac{1}{E_f + M_N} + \frac{1}{E_i + M_N} \right) i \quad (k - q)q \quad ;
\end{aligned} \tag{17}$$

The subscripts  $a$  ( $= 1, 2, 3, 4$ ) and  $v$  ( $= 0, 1$ ) denote the helicity elements of the amplitude in the helicity space.

It turns out to be impossible to extrapolate the theory of Pomeron exchange from high energy regions ( $E >> 10$  GeV) down to the regions  $3.0 < E < 6.7$  GeV [23], with the same normalization factor  $\alpha_0$ . The cross sections will be over-estimated if the same normalization factor is used in the low energy region. Thus, another normalization factor must be taken for the quark-Pomeron coupling  $\alpha_s$  at the nucleon-Pomeron vertex. We derive the normalization factor by fitting the data from Ref. [23] at  $E = 6.45$  GeV. It gives the s-quark-Pomeron coupling strength  $\alpha_s = 1.27$  GeV $^{-1}$  (for instance, in Ref. [5]  $\alpha_s = 1.5$  GeV $^{-1}$  has been adopted). Qualitatively, the change of the normalization factor can be explained by the non-perturbative dressing of the quark-gluon vertex required by the Slavnov-Taylor identity, which introduces a nontrivial flavor dependence at the vertex [5]. In other words, we have made the assumption

that the contribution from the flavor dependence of the quark-Pomeron vertex can be absorbed into the constant  $s_0$  ( $= 0$ ) [2,5]. Concerning the other parameters, we adopt the same values as used in Ref. [5]:  $\alpha_s = 0.08$ ,  $\alpha_0 = 0.25$  GeV $^{-2}$ ,  $m_0 = 1.2$  GeV.

### 2.3 t-channel $\pi^0$ exchange

The Lagrangian for the  $\pi^0$  exchange has the following form:

$$L_{NN} = ig_{NN} \bar{\psi}_5 (\psi_5) \quad (18)$$

for the  $NN$  coupling vertex, and

$$L_{\pi^0} = e_N \frac{g_{\pi^0}}{M} \bar{\psi}_A \psi_A \quad (19)$$

for the  $\pi^0$  coupling vertex, where the  $\psi$  and  $\psi^0$  represent the  $\psi$  and  $\psi^0$  fields, respectively,  $A$  denotes the electromagnetic field,  $\epsilon$  is the Levi-Civita tensor, and  $M = 1.02$  GeV is the mass of the meson. The  $g_{NN}$  and  $g_{\pi^0}$  in Eqs. (18) and (19) denote the coupling constants at the two vertices, respectively. Therefore, the transition amplitudes of the t-channel  $\pi^0$  exchange have the following expression:

$$M_T(\pi^0) = \frac{e_N g_{NN} g_{\pi^0}}{2M} \frac{h}{(t - m^2)} \epsilon^{ijk} (q^i \epsilon_{jk} + !k^i (q^j \epsilon_{jk})) \frac{i}{A e^{\frac{(q-k)^2}{6^2}}} \quad (20)$$

for the transverse transition, and

$$M_L(\pi^0) = \frac{e_N g_{NN} g_{\pi^0}}{2M} \frac{M}{(t - m^2)} \frac{1}{\vec{q} \cdot \vec{j}} (q^i k^j - q^j k^i) A e^{\frac{(q-k)^2}{6^2}} \quad (21)$$

for the longitudinal transition, where  $!k$  in the transition amplitudes denotes the energy of the photon with momentum  $k$ , and the vector  $A = \frac{q}{E_f + M_N} + \frac{k}{E_i + M_N}$ . The momentum transfer squared is  $t = (q - k)^2 = M^2 - 2k \cdot q$ . The factor  $e^{\frac{(q-k)^2}{6^2}}$  in Eqs. (20) and (21) plays a role like the form factor for both  $NN$  and  $\pi^0$  vertices. It comes out naturally in the harmonic oscillator basis since the nucleon is treated as a 3-quark system which is non-point-like. Therefore, the expansion of the internal motion gives such a momentum-dependent factor. The constant  $A$  in this form factor is treated as a parameter.

Since  $\Gamma$  describes the combined form factor for both  $N\bar{N}$  and  $\Delta\bar{N}$  vertices, we don't expect it has the same value as  $\Gamma = 410$  MeV which only corresponds to the  $N\bar{N}$  vertex in the s- or u-channel. We adopt the following values for the couplings:

$$g_{N\bar{N}}^2 = 4 = 14; g_{\Delta\bar{N}}^2 = 0.143; \Gamma = 300$$

It is worth noting that the inclusion of the t-channel  $\Delta^0$  exchange might result in a double-counting problem due to duality arguments. However, in the following sections, one can see that the  $\Delta^0$  exchange plays a quite negligible role in the  $\Delta$  meson photoproduction, which suggests that the duality hypothesis gives little constraint on this process. Since the duality problem is beyond a phenomenological study, we present results with or without the  $\Delta^0$  exchange to illustrate the effects in the following studies.

### 3 Observables and discussion

In this work, we limit the discussion to the low energy region where the effects from nucleon resonances are expected to play a role in the reaction mechanism of the  $p + p$  process.

#### 3.1 Cross-section

As discussed in subsection 2.2, the picture of quark- $\pi$  meson couplings is consistent with each other in the Pomeron exchange and in the s- and u-channel mechanisms. The analogy between the above two vertices leads to the value  $a = 0.16$ . However, this approach does not put any constraint on the parameter  $b^0$  ( $b - a$ ), which contributes in the large  $|t|$  region in the s- and u-channel.

We have attempted to extract the values of the  $a$  and  $b^0$  parameters by fitting the differential cross section data. The result is :

$$a = 0.035 \quad 0.166; \quad b^0 = 0.338 \quad 0.075;$$

First, let us mention that this result should be taken with caution since we fit the data at forward angles whereas the influence of  $a$  and  $b^0$  is at large angles. However, this result shows that parameter  $b^0$  is well constrained while the constraint on parameter  $a$  is loose. For  $a$ , rather than a precise value, the result provides a range which is consistent with the value reported in Section 2.2. In the s- and u-channel, the parameter  $a$  reflects the vector coupling of  $uu$  or  $dd$  which should be suppressed by the OZI rule. In the above fitting, the small central value of  $|a| = 0.035$  shows some hints from such a suppression. However, recalling that one of our motivations is to investigate the sensitivities of the polarization observables to the small s- and u-channel contributions, we have to take into account the large uncertainty in parameter  $a$ . In other words, larger value for  $a$  is to give the upper limit of the sensitivities of the polarization observables. For  $b^0$ , the result favors a negative sign. Also, with the same motivation, we will present in the following the results for all the phase sets for  $a$  and  $b^0$  to provide a complete and systematic understanding of the role played by the s- and u-channel contributions.

We hence fix the absolute values of the two parameters at the following values compatible with the above ranges:

$$|a| = 0.15; \quad |b^0| = 0.3; \quad (22)$$

As we will see below, these values allow to reproduce well enough the existing data on the cross section as well as the density matrix elements.

Notice that:

The extreme value  $|a| = 0.15$  with different signs will show the maximum sensitivities of various observables to the resonance contributions. The OZI suppression considerations are discussed in section 3.5.

Since we always have the combination of the parameters  $b/a$  in the amplitudes, we define  $b^0/b/a$ , and use  $a$  and  $b^0$  as the two parameters for the quark-vector-meson coupling.

Once the signs of the two parameters  $a$  and  $b^0$  are determined, the phases between the s-, u-channel amplitudes, Pomeron, and  $\rho^0$  exchanges can be fixed.

The above values, Eq. 22, are smaller than those estimated in Ref. [14]. The reason is that no Pomeron exchange was included there, therefore, the contributions from the non-diffractive effective Lagrangian were overestimated.

In Fig. 2, the results of our calculations for the differential cross section at  $E = 2.0$  GeV are shown. The  $\rho^0$ -exchange contribution is small and limited to low momentum transfers. The s- and u-channel resonances produce an almost flat contribution which becomes dominant roughly above  $|t| = 1$  (GeV/c)<sup>2</sup>. For the Pomeron exchange, we show results at two energies (2.0 and 6.45 GeV). The Pomeron exchange is the dominant contribution for  $|t| > 0.5$  (GeV/c)<sup>2</sup>, and shows a soft dependence on the energy. As seen in Figs. 2(b)–(d), the differential cross section shows basically no sensitivity to the signs of the couplings  $a$  and  $b^0$ .

We also present predictions for the total cross section (Fig. 3). In spite of large uncertainties in the data, the theory-experiment comparison shows that our model reproduces consistently the dominating diffractive contributions in the whole phase space spanned by the data. Moreover, the almost energy-independent behavior of the meson photoproduction process is reproduced correctly in the model. From these considerations, we conclude that our treatment of the diffractive contribution is realistic enough. As emphasized in Introduction, based on such a reliable treatment, we can now investigate the role of the non-diffractive meson production mechanism in the  $p + p$  process.

In the case of differential and total cross sections, the non-diffractive effects turn out to be small. However, as we will see below, such small effects can be amplified in polarization observables. The rest of this section is devoted to the polarization observable asymmetries where the differential cross section enters in the denominator.

### 3.2 Single polarization asymmetries

The beam polarization asymmetry at  $E = 2.0$  GeV is shown in Fig. 4. Comparing the Pomeron exchange (dashed curve in Fig. 4 (a)) with the Pomeron

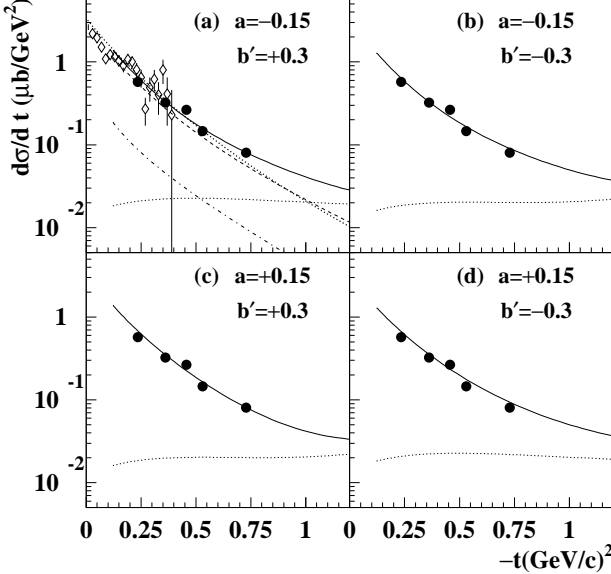


Fig. 2. Differential cross section at  $E = 2.0$  GeV as a function of momentum transfer ( $-t$ ) for  $p \gamma \rightarrow p$ . Data at  $E = 2.0$  GeV (full circle) are from Ref. [26], and at  $E = 6.45$  GeV (diamond) from Ref. [23]. The curves are: i)  $\rho^0$ -exchange (dot-dashed); ii) s- and u-channel contribution (dotted); iii) Pomeron exchange (dashed), and iv) contributions from i) to iii) (full curves). The Pomeron exchange at  $E = 6.45$  GeV is also depicted (heavy dotted curve in (a)). Contributions from the Pomeron and  $\rho^0$  exchanges (independent of  $a$  and  $b^0$ ) are only shown in (a).

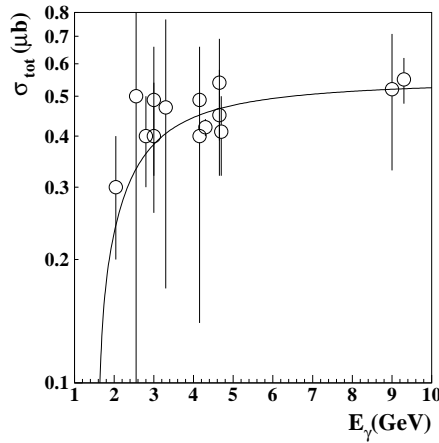


Fig. 3. The total cross section for  $p \gamma \rightarrow p$ . The curve is the prediction of our full calculation and the data are from Ref. [27].

plus  $^0$  exchange (dotted curve in Fig. 4 (a)), we find that the contribution from  $^0$  exchange is negligible. The s- and u-channel contributions are split by the Pomeron exchange, due to the interference term  $s$ , increase the magnitude of the observable by about a factor of 3 around 110° and produces a sign change above 150° (dot-dashed curve in Fig. 4 (a)). The three mechanisms together produce the full curves in Fig. 4 (a) and (b). We present the results for the four phase sets in Fig. 4 (b) for comparison.

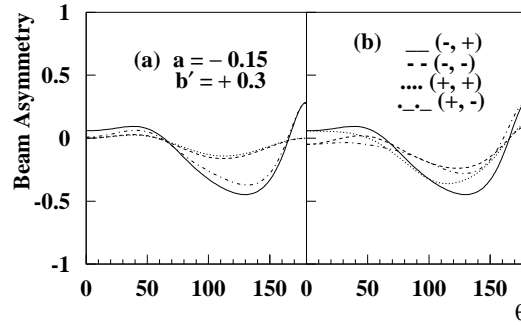


Fig. 4. The polarized beam asymmetry at  $E = 2.0$  GeV with different phase signs. The curves in (a) stand for: Pomeron exchange (dashed), Pomeron and  $^0$  exchanges (dotted), Pomeron exchange and resonance contributions (dot-dashed), and the full calculation including all three components with  $a = -0.15$ ,  $b^0 = 0.3$  (full). In (b), the results of our full calculations for the four  $(a, b^0)$  sets are depicted.

In Fig. 5 predictions for the target polarization asymmetry  $T_{P_N \gamma T}$ , due to the same mechanisms discussed above in the case of the observable are reported.

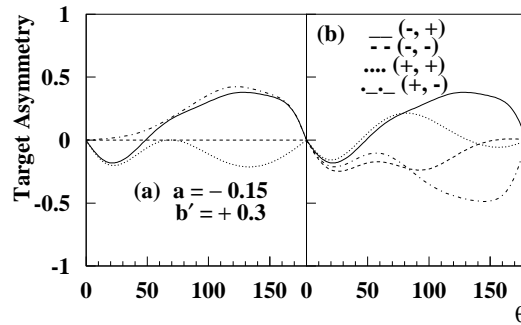


Fig. 5. Same as Fig. 4, but for the polarized target asymmetry.

Here, we wish to emphasize that the helicity amplitude structure of the observable differs drastically from those of the other single polarization observables. As summarized in Appendix, the observable is a bilinear combination of real-real or imaginary-imaginary parts, while the other three single polarization observables depend on real-imaginary couples. Moreover, the Pomeron exchange amplitude is treated purely imaginary in this model while that of

the  $^0$  exchange is purely real. Therefore, the pure Pomeron exchange term, leads to a zero target asymmetry (dashed curve in Fig. 5 (a)), while adding the  $^0$  exchange produces non-zero effects, especially at large angles (dotted curve in Fig. 5 (a)). We find that a large cancellation arises between the longitudinal and transverse parts of the asymmetry, which produces a nearly zero asymmetry at  $\theta = 65^\circ$ . This structure is independent on the relative phase between the Pomeron exchange and the  $^0$  exchange amplitudes, since the Pomeron exchange amplitude is purely imaginary and the  $^0$  exchange is purely real, therefore, the phase change will only give an overall sign to the dotted curve in Fig. 5 (a).

The Pomeron plus resonances contributions (dot-dashed curve in Fig. 5 (a)) gives even a larger asymmetry in magnitude, with opposite sign for backward angles, than the Pomeron plus  $^0$  exchange does. The full calculation (full curves in Fig. 5 (a) and (b)) shows a minimum around  $20^\circ$  due to  $^0$  exchange and a maximum around  $130^\circ$  generated by the resonance terms. In both cases the Pomeron exchange plays an amplifying role in the predicted asymmetries. It shows that the target polarization asymmetry is governed mainly by the resonance contributions at large angles. For comparison, we also present the results with phase changes in Fig. 5 (b).

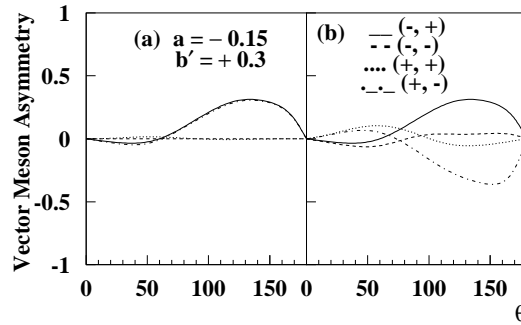


Fig. 6. Same as Fig. 4, but for the polarized vector meson asymmetry.

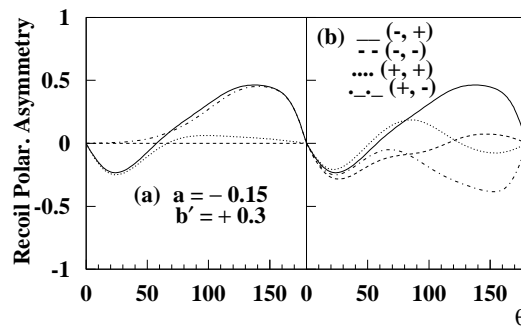


Fig. 7. Same as Fig. 4, but for the recoil polarization asymmetry.

In Fig. 6, the vector polarization observable  $P_V$  for the vector meson polarization is depicted. Here, the combined Pomeron and  $\rho^0$  exchanges produce a very small positive asymmetry. The dominant effect is therefore due to the contributions from the s- and u-channel resonances once again amplified by the Pomeron exchange (dot-dashed curve in Fig. 6(a)).

Finally, we show in Fig. 7 the recoil polarization asymmetry  $P_{N^0}$ .

To summarize the main features revealed by the single polarization observables:

The Pomeron exchange mechanism turns out to be an efficient amplifier for the mechanisms suppressed in the cross sections.

Although the influence of the  $\rho^0$  exchange can be amplified in some polarization observables, it plays in general a rather minor role. Therefore, this might imply that the double-counting from duality (if it exists) is negligible.

The nodal structure of the observables depends (in some cases heavily) on the signs of the two couplings  $a$  and  $b^0$ .

The s- and u-channel resonances produce significant effects. The most favorable phase space region depends on the signs of the couplings  $a$  and  $b^0$  (Figs. 4(b), 5(b), 6(b), and 7(b)).

### 3.3 Double polarization asymmetries

Given the availability of polarized beam and polarized target, we now concentrate on the beam-target (BT) double polarization asymmetry. A motivation in investigating this observable is that a recently developed strangeness knock-out model [11] suggests that a small  $s\bar{s}$  component (5%) in the proton might result in large asymmetries (25-45%) in the BT observable at small angles. However, since the resonance contributions have not been taken into account there, an interesting question is: if contributions from the s- and u-channel can produce a significant double polarization asymmetry without introducing strangeness component or not.

Our predictions are shown in Fig. 8. The Pomeron exchange alone (dashed curve in (a)), gives a negative asymmetry which increases in magnitude from forward to backward angles where the largest asymmetry is about 40%. The  $\rho^0$  exchange (dotted curve in (a)) diminishes slightly the asymmetry, while the resonances contributions (dot-dashed curve in (a)) enhances it. The full calculation leads finally to a decreasing behavior, going from almost zero at forward angles to -0.7 at 180°. This result (full curve in Fig. 8(a) and (b)) is obtained with  $a = 0.15$  and  $b^0 = +0.3$ . The backward angle effects are also large in the case of  $a = +0.15$  and  $b^0 = -0.3$  (dot-dashed curve in Fig. 8(b)). The situation becomes very different for the couplings sets with the

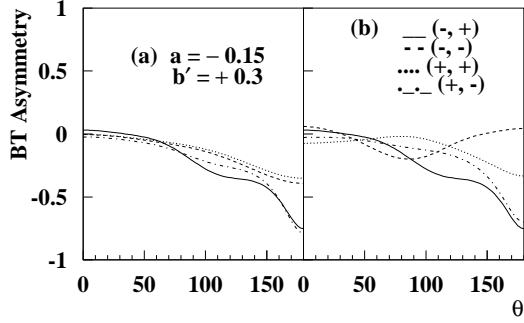


Fig. 8. Same as Fig. 4, but for the polarized beam-target asymmetry. The heavy dotted curve in (a) is given by the full calculation with  $a = -0.15$ ,  $b^0 = +0.3$ .

same signs: the effect is suppressed for  $a = +0.15$  and  $b^0 = +0.3$  (dotted curve in Fig. 8(b)), and the shape changes drastically for  $a = -0.15$  and  $b^0 = 0.3$  (dashed curve in Fig. 8(b)). The latter set produces (almost) vanishing values at extreme angles. The common feature to all four sets is that the beam-target asymmetry is small at forward angles.

### 3.4 Density matrix elements

In this subsection, the density matrix elements are investigated in the helicity system. Data for the density matrix elements at low energies [23] are still very sparse: measurements have been carried out only in the small  $t$  region ( $q^2 < 20$ ) at  $E = 5.165$ , and  $6.195$  GeV, where the Pomeron exchange dominates over other non-diffractive processes. In Fig. 9 the solid curve is the

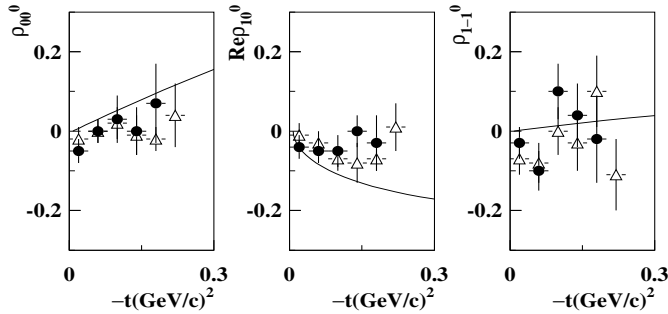


Fig. 9. Theoretical predictions for the density matrix elements at  $E = 5.165$  GeV. Data at  $E = 5.165$  GeV (full circle) and at  $E = 6.195$  GeV (triangle) are from Ref. [23].  $t = 0.3$   $(\text{GeV}/c)^2$  corresponds to  $q^2 = 22$ .

result of our calculation at  $E = 5.165$  GeV. At  $E = 6.195$  GeV, the results are not significantly different within this momentum transfer region, so, we do not show them here. Theory-data comparison shows again the character of

di ractive dominance in the small  $t$  region, and the Pomeron exchange (other amplitudes are included but negligible at this energy region) reproduces well enough the data for the three density matrix elements  $\rho_{00}^0$ ,  $\text{Re } \rho_{10}^0$  and  $\rho_{11}^0$ .

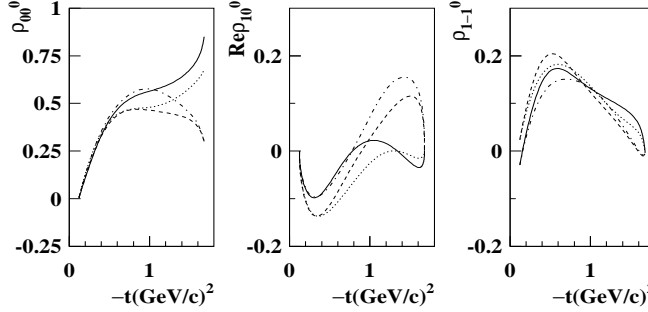


Fig. 10. Density matrix elements predicted at  $E = 2.0$  GeV with phase changes for (a;  $b^0$ ): solid ( ; + ), dashed ( ; - ), dotted ( + ; - ), and dot-dashed ( + ; + ) curves.

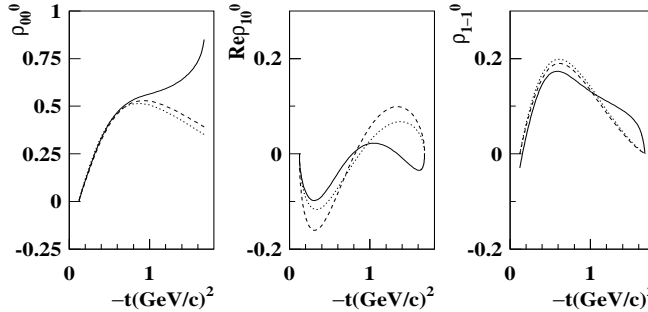


Fig. 11. Density matrix elements predicted at  $E = 2.0$  GeV with  $a = 0.15$ ,  $b^0 = 0.3$ . The curves stand for: pure Pomeron exchange (dashed), Pomeron plus  $\rho^0$  exchanges (dotted), and full calculation (full).

In Fig. 10, our predictions for the three density matrix elements at  $E = 2.0$  GeV are presented for di erent  $a$  and  $b^0$  phase sets. In Fig. 11, contributions from only the Pomeron exchange (dashed curve), Pomeron plus  $\rho^0$  exchanges (dotted curve), and both exchanges plus the resonance contributions (full curve) are shown. The density matrix elements appear to be quite sensitive to the non-di ractive s- and u-channel contributions. Also, the phase changes produce signi cant e ects in the large  $t$  region. However, in the forward di rection, the density matrix elements are not sensitive neither to the non-di ractive resonance e ects nor to the phase changes.

### 3.5 OZI suppression effects

As mentioned in subsection 3.1, the numerical results discussed there are obtained for  $|a| = 0.15$ , which corresponds to no OZI suppression. Here, we report on the manifestations of such a suppression in the absence of OZI evading mechanisms. The OZI rule would imply a parameter value smaller by roughly one order of magnitude. To single out possible manifestations of the OZI suppression, we compare the numerical results for different observables for  $|a| = 0.15$  and  $a = 0.015$ .

As already discussed, from the Pomeron-photon analogy picture, no constraint can be imposed on the other free parameter,  $b^0$ . However, the value  $b^0 \approx 0.3$  could indicate an OZI suppression: the value extracted here is about one order of magnitude smaller than  $b^0 = 2.5$  used in the  $\pi$  and  $\eta$  mesons photoproduction [14].

In Fig. 12, our results for three single polarization (beam, target, and vector meson), as well as the beam-target double polarization asymmetries are depicted. The polarized beam asymmetry shows little sensitivity to the phase of  $a$ , but depends significantly on the absolute value of this parameter. This observable is hence very appealing to study the OZI suppression effects and/or the related evading mechanisms. In the target and vector meson polarization asymmetries, the  $a$ -dependent terms come in basically in the interference terms and are mostly sensitive to the phase of this parameter. The beam-target double polarization asymmetry, turns out to result from cancellations among the helicity amplitudes, except at extreme backward angles where strong dependences on both the phase and magnitude of  $a$  show up. This explains the large asymmetries (solid curve in Fig. 12) found for a small value of the coupling  $a$ . The curves without  $s$ - and  $u$ -channel contributions (i.e. only Pomeron plus  $^0$  exchange) are also shown for comparison.

Density matrix elements are shown in Fig. 13. The  ${}^0_{00}$  above  $|a| = 1$ .  $(\text{GeV}/c)^2$  shows a possibility to determine both the phase and the size of the parameter, while the  $\text{Re} {}^0_{10}$  depends strongly on the phase. The  ${}^0_{11}$  turns out to be dominated by the non-resonant terms (see Fig. 11).

The results presented here show clear sensitivity of some of the observables to the nucleon resonance contributions even in the presence of the OZI suppression mechanism.

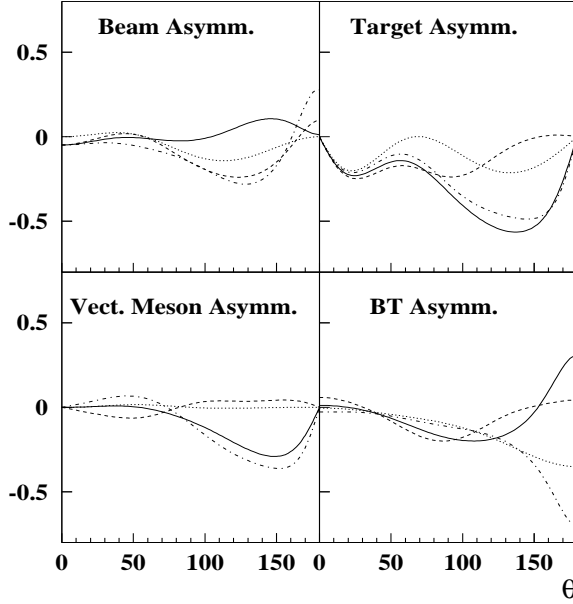


Fig. 12. Single and double polarization observables predicted at  $E = 2.0$  GeV with  $b^0 = 0.3$ . The curves stand for: Pomeron plus  $\rho^0$  exchanges (dotted), and full calculation for  $a = 0.15$  (dot-dashed),  $a = 0.15$  (dashed), and  $a = 0.015$  (solid).

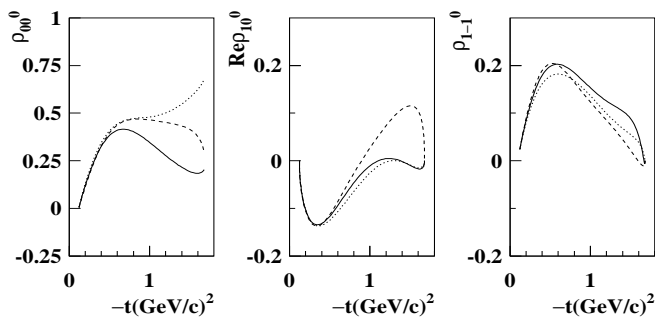


Fig. 13. Density matrix elements predicted at  $E = 2.0$  GeV with  $b^0 = 0.3$ . The curves stand for: full calculation for  $a = 0.15$  (dotted),  $a = 0.15$  (dashed), and  $a = 0.015$  (solid).

## 4 Pomeron gauge invariance effects

This section is devoted to investigate the sensitivity of the Pomeron exchange model to the various gauge-fixing schemes. This question arises from the fact that the Pomeron exchange is introduced phenomenologically to account for the diffractive behavior at small angles. However, at large angles, the description of the Pomeron structure is still an unsolved question. Here, we limit our discussion to the effects due to the different gauge-fixing schemes and the non-gauge-invariant one.

In Fig.1, the loop tensor is derived by supposing that the constituent quarks carry half of the momentum of the vector meson:

$$\begin{aligned} t(k; q) = & 2k \cdot g - \frac{2}{q^2} k \cdot q \cdot q - 2g \cdot (k \cdot q \cdot \frac{k \cdot q}{q^2}) \\ & + 2(k \cdot q) (g - \frac{q \cdot q}{q^2}); \end{aligned} \quad (23)$$

where the second line violates gauge invariance. Taking into account that at the photon and vector meson vertices,  $k^2 = 0$  and  $q^2 = 0$ , one finds that the contributing terms are:

$$t(k; q) = 2k \cdot g - 2g \cdot k - 2q \cdot g : \quad (24)$$

We note the above non-gauge-invariant Pomeron amplitude as  $t_0$ . In Ref.[11], two schemes for restoring gauge invariance are employed. We refer reader to Ref.[11] for detailed discussion of how to derive the gauge-fixing terms, and skip to the final forms of the loop tensor.

In this work we have adopted the gauge-fixing scheme which gives the loop tensor as the following:

$$\begin{aligned} t(k; q) = & (k + q) \cdot g - 2k \cdot g \\ & + 2 \frac{h}{k} k \cdot g + \frac{q}{q^2} (k \cdot q g - k \cdot q \cdot q \cdot k) \\ & - \frac{k^2 q}{q^2 k} (q^2 g - q \cdot q) + (k \cdot q) \cdot g : \end{aligned} \quad (25)$$

The contributing terms can be easily derived and are given by Eq. (13). Here we name this gauge-fixing scheme as  $t_1$ .

Another gauge-fixing scheme gives the contributing terms as:

$$t(k; q) = (k + q) \cdot g - k \cdot g - q \cdot g : \quad (26)$$

where those terms which do not contribute are omitted for brevity. We note this gauge-fixing scheme as t2.

Comparing these three kinds of Pomeron exchanges:  $t_0$ , non-gauge-invariant;  $t_1$  and  $t_2$ , gauge-invariant, one finds that these different Pomeron exchanges will produce different behaviors. However, one can identify the two terms which are different between the three Pomeron amplitudes:  $q$  and  $q^2$ , and finds that they generally play a role as a higher order contribution at forward angles. For  $q^2$  we write explicitly the non-relativistic expansion as follows:

$$M_T = q \frac{k}{E_i + M_N} + q \frac{i(q-k)}{E_f + M_N} \frac{i(q-k)}{E_i + M_N}^{\#}; \quad (27)$$

and

$$M_{\text{L}} = q \frac{i^2}{E_f + M_N} + ! \left( \frac{q^2}{E_f + M_N} + \frac{q}{E_i + M_N} \right)^{\#} \frac{i(q-k)}{E_i + M_N}; \quad (28)$$

where  $M_T$  and  $M_L$  represent the transverse and longitudinal transition amplitude, respectively. Also, this term is the one which makes the difference between the two gauge-fixing schemes,  $t_1$  and  $t_2$ . However, at forward angles, this term becomes small and vanishes since  $q$  has almost the same direction as  $k$  in the forward scattering, therefore, the product  $q \cdot k$  becomes very small. Qualitatively, we can see that the product of  $q \cdot k$  gives an overall suppression of this term, which guarantees the consistent behavior of the Pomeron exchanges at small angles with different gauge-fixing schemes.

For the second term,  $q^2$ , which is also essential to restore gauge invariance, we find that there is also an overall suppression of the longitudinal amplitude from  $q^2$  in the forward direction:

$$M_{\text{L}} = q \frac{i^2}{E_f + M_N} + ! \left( \frac{q^2}{E_f + M_N} + \frac{q}{E_i + M_N} \right)^{\#} \frac{i(q-k)}{E_i + M_N}; \quad (29)$$

Note that in Eqs. 28 and 29, except for the first term in the first line, the other terms are identical. Therefore, the substitution of Eq. (28) and (29)

into scheme t2 in the longitudinal amplitude for the two terms gives,  $M_L = M_q = 0$ , which is obviously suppressed in the forward direction.

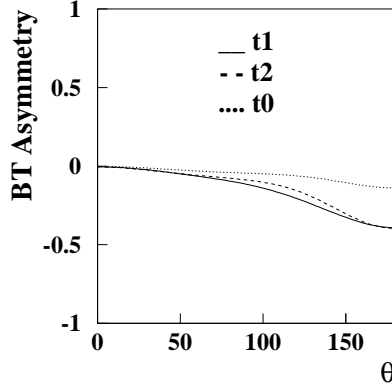


Fig. 14. Beam-target asymmetry for different Pomeron exchange amplitudes. The non-diactive contributions have been switched off.

For the transverse amplitude of the  $q$  term, the explicit expression is:

$$M_T = \left( 1 + \frac{q^2}{E_f + M_N} + \frac{q \cdot k}{E_i + M_N} \right) \frac{i \cdot (q \cdot k)}{E_i + M_N}; \quad (30)$$

where the second term is suppressed by  $(q \cdot k)$  in the forward direction. However, for the first term in the above equation, the only suppression comes from the relatively small momentum of the massive meson.

In Fig.14, the beam-target asymmetry for different Pomeron exchanges (with only the diactive Pomeron contribution) are presented. It shows that they consistently converge to small asymmetry at forward angles while at large angles the asymmetry is quite sensitive to the particular Pomeron structure. The solid curve is given by the t1 gauge-fixing scheme and the dotted curve by t2. The non-gauge-invariant Pomeron t0 (dashed curve) has a similar behavior as t1. Therefore, a question arising from this result is that "if the non-diactive contributions are taken into account, the polarization asymmetries are sensitive to the Pomeron structure or not?" Since the Pomeron structure at large angles is unknown, a gauge-dependent Pomeron interference at large angles might make the asymmetry predictions misleading. To investigate this aspect, we calculate the polarization asymmetries with diactive Pomeron exchanges given by t0, t1 and t2, and the results are presented in Fig. 15 and 16. Comparing the results given by the diactive Pomeron exchanges, we find

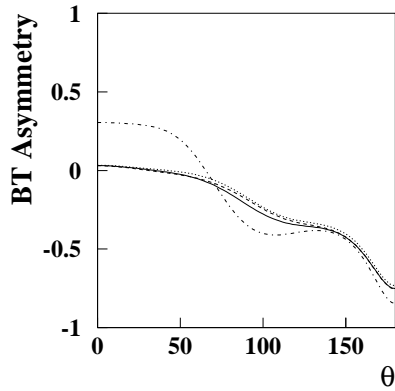


Fig. 15. Beam-target asymmetries with all the contributions taken into account. The Pomeron exchange is given by  $t_1$  (full),  $t_2$  (dashed), and  $t_0$  (dotted). The dot-dashed curve represents the asymmetry without the Pomeron exchange.  $a = 0.15$ ,  $b^0 = 0.3$  have been adopted for the s- and u-channel contributions.

that they have very similar behaviors in the polarization asymmetries observables which means that the asymmetries are not sensitive to the Pomeron structures when the non-diactive contributions are taken into account. In other words, although different gauge-fixing schemes are introduced for the Pomeron exchange terms, they produce a quite gauge-independent interference in the polarization asymmetries, which means that the asymmetries can be considered mainly determined by the non-diactive contributions. Since the asymmetries predicted at large angles have little dependence on the Pomeron exchange models, the experimental observation can provide a direct test of the model for the s- and u-channel reactions.

We also present the asymmetries produced by the non-diactive contributions (dot-dashed curves) in Fig. 15 and 16, i.e. the interference just between the  $^0$  exchange and the s- and u-channel contributions. It shows that in the vector meson, target and recoil polarization asymmetries, the influence from the Pomeron exchange produces dramatic changes to the asymmetries throughout all the angular region, while in the beam-target and beam polarization asymmetry, we find that the interference from the Pomeron exchange is important at small angles but not so significant at large angles. These features can be explained by the helicity structures of these observables and the forward peaking character of the Pomeron exchange. For the vector meson, target and recoil polarization asymmetry observables, the asymmetry is produced by the summation over the products between the real helicity elements and the imaginary ones, which means that the small imaginary amplitude of the Pomeron exchange at large angles can be amplified by the dominating non-diactive real amplitudes. However, for the beam-target polarization asymmetry and the polarized beam asymmetry, the asymmetry is given by

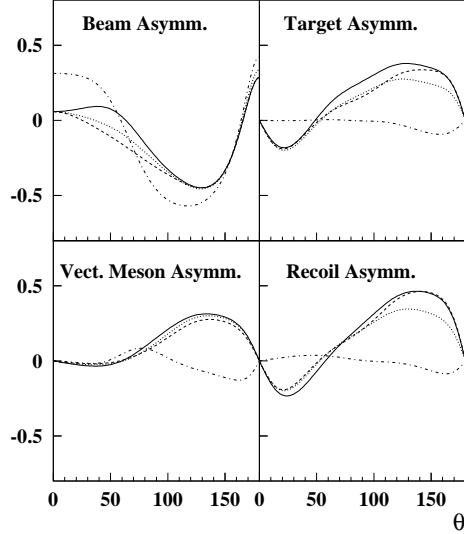


Fig. 16. Single asymmetries with all the contributions taken into account. The curves have the same meanings as in Fig. 15.

the summation over the products between imaginary helicity elements, or between the real ones, which means that at large angles, the effects from adding a small value from the Pomeron exchange are negligible. It should be noted that dot-dashed curves for the asymmetries from the non-diffractive contributions in Fig. 15 and 16 have only theoretical meaning since the dominating diffractive contribution must be involved at small angles.

In summary, although the Pomeron exchange can have different structures due to the different gauge-fixing schemes, it does not influence significantly the polarization observables at large angles. Therefore, the main feature of an asymmetry can be regarded as depending more on the non-diffractive contributions rather than on the particular Pomeron structure.

## 5 Configuration mixing effects

In the previous section, the wave functions for the s- and u-channel resonances are assumed to have the exact  $SU(6) \times O(3)$  symmetry. The present data on the  $\eta$  meson are too scarce to allow a study of possible deviations from this exact symmetry. However, because the isospin of the  $\eta$  meson is the same as that of the  $\pi$  meson, the formalism for the s- and u-channel contributions from the effective Lagrangian should be the same as that of the  $\pi$  production in the  $SU(3)$  isospin symmetry limit. The major difference between the  $\pi$  and  $\eta$  meson production is the mechanism of generating  $u(d)$  and  $\bar{u}(\bar{d})$  quarks for the  $\pi$  production and the  $s\bar{s}$  quarks for the  $\eta$  production which is suppressed by the OZI rule. On the other hand, since large  $SU(3)$  flavor symmetry violation exists between the constituent quarks,  $u$ ,  $d$ , and  $s$ , which results in the large mass splitting between the non-strange vector mesons ( $\pi$  and  $\eta$ ) and the strange ones ( $K$  and  $\bar{K}$ ), we do not expect that with the same set of parameters as in Refs. [13,14] we can reasonably describe the differential cross section in the large momentum transfer region. In fact, relatively smaller values are adopted in this case, and they reflect some effects from the OZI suppression. To take into account the configuration mixing in the quark model based on the  $SU(6) \times O(3)$  symmetry, a reasonable treatment is to extract the symmetry breaking coefficients by using the  $\eta$  meson data. This procedure is explained in the following subsection. Subsequently, these results are used in studying the relevant observables in the case of the  $\eta$  meson photoproduction.

### 5.1 Configuration mixing coefficients extraction via the process $p + \eta \rightarrow p + p$

In the  $SU(6) \times O(3)$  symmetry limit, the only adjustable parameters are  $a$  and  $b$ . To investigate the symmetry breaking effects in the  $\eta$  meson photoproduction, one introduces [17] a new set of parameters  $C_R$ , and the following substitution rule for the helicity amplitudes of the resonances  $R$ :

$$h_{a_v}^J \rightarrow C_R h_{a_v}^J; \quad (31)$$

In the process under study, a priori eight nucleonic resonances can contribute. As mentioned above, the amount of available data on the  $\eta$  meson is too small to allow a fitting procedure with 8 to 10 free parameters. Given that the same resonances are present in the  $\pi$  photoproduction reaction, the strategy adopted here is to extract the above configuration mixing parameters ( $C_R$  in Eq. (31)) from the  $p + \eta \rightarrow p + p$  channel. For this purpose, using the MINUIT code [24], we have fitted the recent data from the SAPHIR collaboration [25] on the  $\eta$  photoproduction; see Table 2. In Fig. 17, the results for the latter channel are depicted. The full curve (S1) is obtained by fitting the data with two adjustable

Table 2

Values of the parameters  $a$  and  $b^0$  (S1) and the configuration mixing coefficients (S2) extracted from fitting the SAPHIR data [25] for  $p \neq p$ , as well as the reduced  $\chi^2$ s.

Notation	S1		S2	
$a$	-1.58	0.07	-1.58	
$b^0$	1.08	0.38	1.08	
$C_{S_{11}}(1535)$	1.	2.50	0.34	
$C_{D_{13}}(1520)$	1.	-0.97	3.23	
$C_{P_{13}}(1720)$	1.	1.14	0.69	
$C_{F_{15}}(1680)$	1.	2.29	0.47	
$C_{P_{11}}(1440)$	1.	2.50	3.16	
$C_{P_{11}}(1710)$	1.	2.50	4.26	
$C_{P_{13}}(1900)$	1.	0.51	3.77	
$C_{F_{15}}(2000)$	1.	4.66	4.66	
$\chi^2_{\text{d.o.f}}$	1.59		1.46	

parameters  $a$  and  $b^0$ , while all configuration mixing coefficients have been put to 1, i.e. their SU(6) O(3) symmetry values (second column in Table 2). The dotted curve in Fig. 17 comes from a second minimization procedure where the parameters  $a$  and  $b^0$  have been fixed to their S1 configuration values and all eight configuration mixing coefficients have been extracted (third column in Table 2) by fitting the same data base.

Here we wish to make a few comments on the results reported in Table 2 and Fig. 17. In the S1 configuration, the values of the parameters  $a$  and  $b^0$  are extracted with small enough uncertainties to fix their relative phases. However, in spite of a significant improvement of the  $\chi^2$ , the uncertainties on the configuration mixing coefficients in S2 are too large to be conclusive, except in the case of two resonances  $P_{13}(1720)$  and  $F_{15}(1680)$ . This uncomfortable situation is due to at least two facts: i) the number of data points is too small compared to the number of free parameters, ii) the differential cross sections do not offer a high selectivity to the underlying reaction mechanism. To go further in such investigations, one needs to measure the polarization observables. However, recalling again that our attention is to investigate the sensitivities of the polarization observables to the configuration mixing, we can reasonably use these coefficients (S2 set in Table 2, which still need to be improved [28]) to explore deviations from the exact SU(6) O(3) symmetry in the  $\pi$  meson photoproduction in the following subsection.

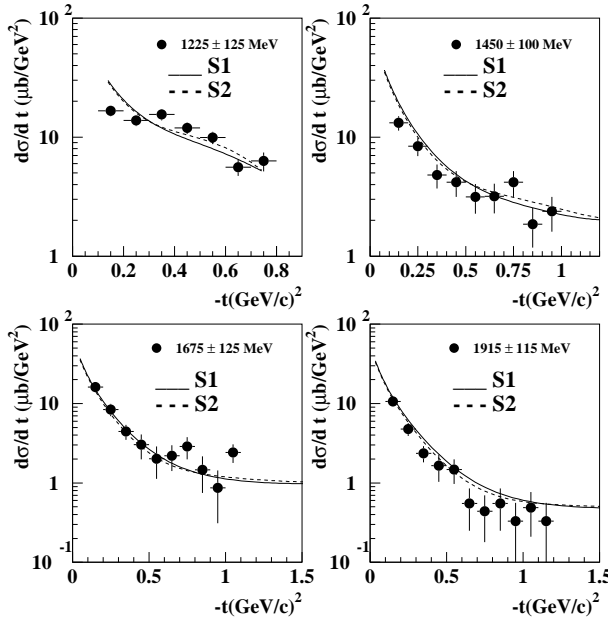


Fig. 17. Differential cross section as a function of momentum transfer ( $-t$ ) for the reaction  $p \rightarrow p$  at four incident photon energies. The data are from the SAPHIR collaboration (Ref. [25]). The curves have been calculated for the central energy values. The full curves correspond to the exact  $SU(6) \times O(3)$  symmetry (set S1 in Table 2), while the dotted curves are obtained by allowing deviation from this symmetry (set S2 in Table 2).

## 5.2 Configuration mixing manifestations in the process $p \rightarrow p$

Using the configuration mixing coefficients above (set S2 in Table 2), we have investigated the sensitivity to these parameters of all the observables reported in Figs. (2) to (11). According to the observable and/or the  $a$  and  $b^0$  sets, one obtains different levels of sensitivities to the configuration mixing effects.

As in the case of the  $\pi^+$  photoproduction, the cross section does not show significant sensitivity to the mechanism under investigation. For the polarization asymmetries, we have singled out the most prominent cases shown in Figs. 18 and 19.

The single polarization asymmetries (18) fall into two families:

- i) The beam ( $\sigma$ ) and vector meson ( $P_V$ ) asymmetries turn out to be most interesting around  $90^\circ$ , where the vanishing asymmetries in the exact  $SU(6) \times O(3)$  symmetry limit, produce sizable asymmetries due to the symmetry breaking.
- ii) The target polarization ( $T$ ) and recoil polarization ( $P_{N^0}$ ) asymmetries are appealing in the backward angles, e.g. around  $150^\circ$  the asymmetries get

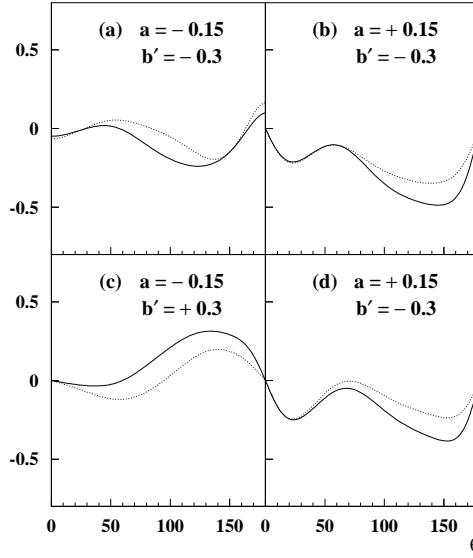


Fig. 18. Configuration mixing effects for the single polarization asymmetries. Figures (a)–(d) represent beam, target, vector meson and recoil polarization asymmetries, respectively. The full curves correspond to the exact  $SU(6) \times O(3)$  symmetry (set S1 in Table 2), while the dotted curves are obtained by allowing deviation from this symmetry (set S2 in Table 2).

roughly doubled with  $a = 0.15$  and  $b^0 = -0.3$ .

In the case of the beam–target double polarization asymmetry, Fig. (19), the sensitivities are observed at large angles.

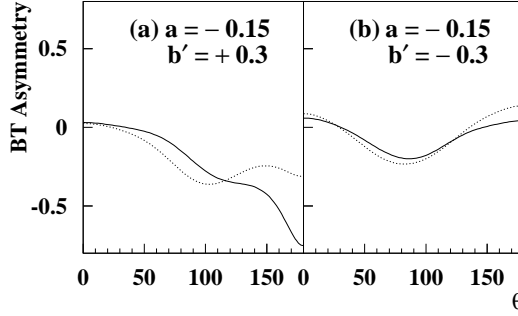


Fig. 19. Same as Fig. 18, but for beam–target double polarization asymmetry.

As a brief summary for the section, the result shows that, generally, the configuration mixings produce significant effects at large angles while at forward angles the polarization asymmetries are not sensitive to the mixings.

## 6 Conclusions

In this paper we have investigated the reaction  $p + p$  in the region close to threshold ( $E_{\text{thres}} = 1.57$  GeV). The known dominant di ractive process is taken into account via the t-channel Pomeron exchange. The main novelty of our work is the study of the role played by the s- and u-channel intermediate nucleonic resonances. This is done using a quark-model based effective Lagrangian approach. Our formalism includes also the small non-di ractive contribution from the t-channel  $\pi^0$  exchange.

In the first step, the nucleonic resonance effects are investigated in the SU(6)  $\times$  O(3) symmetry limit. In the polarization observables, the small nucleonic resonance contributions produce significant asymmetries at large angles, however, the asymmetries are quite small at forward angles.

Based on the different gauge-fixing schemes for the Pomeron exchange terms, three kinds of Pomeron amplitudes are investigated. It shows that these amplitudes converge to a similar behavior at small angles, but have quite different behaviors at large angles when only the Pomeron exchange contributes. However, with the non-di ractive s- and u-channel contribution taken into account, we find that the asymmetries at large angles are governed by the non-di ractive contribution, therefore, the asymmetries are not sensitive to the di ractive Pomeron exchange amplitudes due to gauge invariance. This gives us the confidence that at large angles the ambiguity arising from the Pomeron structure can be neglected in this model.

Deviations from the exact symmetry are also investigated. It shows that the asymmetries at large angles are quite sensitive to the configuration mixing effects while at small angles the change in the asymmetries is negligible.

In summary, the forward angle polarization asymmetries are almost insensitive to the s- and u-channel nucleonic resonance contributions (as well as to the t-channel  $\pi^0$  exchange). This is an interesting finding, since data at small angles might be able to shed a light on other sources, such as the small  $s\bar{s}$  component in the nucleon. At large angles, significant sensitivities to the phases of the couplings provide insights to the small, but still sizable s- and u-channel resonance contributions. These results hold also in the case of OZI suppression relevance. Finally, Some of the phase sets for those parameters ( $a$  and  $b^0$ ), offer also a test of deviations from the exact SU(6)  $\times$  O(3) symmetry.

Upcoming data from JLAB [29] are expected to allow to disentangle various components of the reaction mechanism investigated here. Confrontation between the present theoretical predictions and data might show the limits of the non-relativistic constituent quark approach presented here and the need for more sophisticated and a fully relativistic formalism.

## Acknowledgments

One of us (Q.Z.) expresses his thanks to IPN-Orsay and the "Bourses de Recherche CNRS-K.C. W O N G" for financial support. Two of us (Q.Z. and B.S.) would like to express appreciations to Zhenping Li for his interest in this work and much encouragement. Q.Z. acknowledges the beneficial discussions with C.Bennhold and W.Kloet.

## Appendix

Generally, the helicity amplitudes can be explicitly written as:

$$H_{av} = H_{av}^r + iH_{av}^i \quad (32)$$

where  $H_{av}^r$  and  $H_{av}^i$  represent the real and imaginary part of the amplitude, respectively. The  $v = 0, 1$  is the helicity of the vector meson. With the and  $1$  matrices given by Ref. [19], the four single and one double polarization asymmetries of the spin observables can be expressed explicitly as the followings:

Polarized photon asymmetry

$$\begin{aligned} &= \frac{1}{2} hH j^4 !^A \mathcal{H} i \\ &= \frac{1}{2} f H_{11}^r H_{41}^r - H_{11}^i H_{41}^i + H_{10}^r H_{40}^r + H_{10}^i H_{40}^i \\ &\quad H_{11}^r H_{41}^r - H_{11}^i H_{41}^i + H_{21}^r H_{31}^r + H_{21}^i H_{31}^i \\ &\quad H_{20}^r H_{30}^r - H_{20}^i H_{30}^i + H_{21}^r H_{31}^r + H_{21}^i H_{31}^i g : \end{aligned} \quad (33)$$

Polarized target asymmetry

$$\begin{aligned} T &= \frac{1}{2} hH j^{10} !^1 \mathcal{H} i \\ &= f H_{1v}^r H_{2v}^i - H_{1v}^i H_{2v}^r + H_{3v}^r H_{4v}^i - H_{3v}^i H_{4v}^r g : \end{aligned} \quad (34)$$

Polarized vector meson asymmetry

$$\begin{aligned} P_v &= \frac{1}{2} hH j^1 !^3 \mathcal{H} i \\ &= \frac{3}{2} f H_{11}^r H_{10}^i - H_{11}^i H_{10}^r + H_{21}^r H_{20}^i - H_{21}^i H_{20}^r \\ &\quad H_{31}^r H_{30}^i - H_{31}^i H_{30}^r + H_{41}^r H_{40}^i - H_{41}^i H_{40}^r g : \end{aligned} \quad (35)$$

Recoil polarization asymmetry

$$\begin{aligned} P_{N^0} &= \frac{1}{2} hH j^{12} !^1 \mathcal{H} i \\ &= f H_{3v}^i H_{1v}^r - H_{3v}^r H_{1v}^i + H_{4v}^i H_{2v}^r - H_{4v}^r H_{2v}^i g : \end{aligned} \quad (36)$$

The explicit expression for the component  $C_{zz}^N$  in the beam-target double polarization asymmetry is given by:

$$\begin{aligned}
 C_{zz}^N &= \frac{1}{2} h H_j^9 \bar{H}^1_i \\
 &= \frac{1}{2} \sum_v f H_{1v}^r H_{1v}^r + H_{1v}^i H_{1v}^i - H_{2v}^r H_{2v}^r - H_{2v}^i H_{2v}^i \\
 &\quad + H_{3v}^r H_{3v}^r + H_{3v}^i H_{3v}^i - H_{4v}^r H_{4v}^r - H_{4v}^i H_{4v}^i g : \quad (37)
 \end{aligned}$$

It is worth noting that the helicity amplitudes can be explicitly related to the density matrices which can be measured in experiments [20].

## References

- [1] T.H. Bauer, R.D. Spital, D.R. Yennie and F.M. Pipkin, *Rev. Mod. Phys.* 50, 261 (1978).
- [2] A. Donnachie and P.V. Landshoff, *Phys. Lett. B* 185, 403 (1987); *Nucl. Phys. B* 311, 509 (1989).
- [3] J.-M. Laget and R. Menendez-Galain, *Nucl. Phys. A* 581, 397 (1995).
- [4] L.P.A. Hackmann, A. Kaidalov and J.H. Koch, *Phys. Lett. B* 365, 411 (1996).
- [5] M.A. Pichowsky and T.-S.H. Lee, *Phys. Lett. B* 379, 1 (1996); *Phys. Rev. D* 56, 1644 (1997).
- [6] R.A. Williamson, *Phys. Rev. C* 57, 223 (1998).
- [7] S.O. Kubo, *Phys. Lett.* 5, 165 (1963);  
G. Zweig, CERN Report TH-412 (1964);  
I. Iizuka, *Prog. Theor. Phys. Suppl.* 37, 21 (1966).
- [8] J. Reifnerother et al., ASTERIX Collaboration, *Phys. Lett. B* 267, 299 (1991);  
M.A. Faessler et al., Crystal Barrel Collaboration, *Phys. At. Nucl.* 57, 1693 (1994);  
V.G. Abbleev et al., OBELEX Collaboration, *ibid.* 57, 1716 (1994); *Phys. Lett. B* 334, 237 (1994).
- [9] E.M. Henley, G. Kraen, S.J. Pollock and A.G. Williamson, *Phys. Lett. B* 269, 31 (1991);  
E.M. Henley, G. Kraen and A.G. Williamson, *ibid. B* 281, 178 (1992).
- [10] J. Ellis, M. Karliner, D.E. Kharzeev and M.G. Sapozhnikov, *Phys. Lett. B* 353, 319 (1995).
- [11] A.I. Titov, Y.Oh and S.N. Yang, *Phys. Rev. Lett.* 79, 1634 (1997);  
A.I. Titov, Y.Oh, S.N. Yang and T.M. Orii, *Phys. Rev. C* 58, 2429 (1998).
- [12] A. Titov, T.-S.H. Lee and H. Toki, *nucl-th/9812074*.
- [13] Q. Zhao, Z.P. Li and C. Bennhold, *Phys. Lett. B* 436, 42 (1998).
- [14] Q. Zhao, Z.P. Li and C. Bennhold, *Phys. Rev. C* 58, 2393 (1998).
- [15] S. Capstick and N. Isgur, *Phys. Rev. D* 34, 2809 (1986).
- [16] Zhenping Li, *Phys. Rev. D* 52, 4961 (1995);  
Zhenping Li, Hongxing Ye, and Minghui Lu, *Phys. Rev. C* 56, 1099 (1997).
- [17] Z.P. Li and B. Saghian, *Nucl. Phys. A* 644, 345 (1998).
- [18] R.G. Moorhouse, *Phys. Rev. Lett.* 16, 772 (1966).
- [19] M.A. Pichowsky, C. Savko and F. Tabakin, *Phys. Rev. C* 53, 593 (1996).

- [20] K . Schilling, P . Seyboth and G . W olf, Nucl. Phys. B 15, 397 (1970).
- [21] Particle D ata G roup, C . C aso et al., Euro. Phys. J. C 3, 1 (1998).
- [22] Zhenping Li, Phys. Rev. D 48, 3070 (1993).
- [23] H .J. Behrend et al., Nucl. Phys. B 144, 22 (1978).
- [24] F . James and M . Roos, Comp. Phys. Comm . 10, 343 (1975).
- [25] F J. K lein, Ph.D . thesis, University of Bonn, Bonn-IR-96-008 (1996); N ew slett. 14, 141 (1998).
- [26] H J. B esch et al., Nucl. Phys. B 70, 257 (1974).
- [27] H R . C rouch et al., Phys. Rev. 156, 1426 (1967);  
 R . E rbe et al., Phys. Lett. B 27, 54 (1968);  
 R . E rbe et al., Phys. Rev. 175, 1669 (1968);  
 M . D avier, Phys. Rev. D 1, 790 (1969);  
 J. B allam et al., Phys. Rev. D 7, 3150 (1973);  
 D P . B arber et al., Z . Phys. C 12, 1 (1982).
- [28] Q iāng Zhao et al., work in progress.
- [29] E S . Sm ith et al., JLAB proposal E 93-022;  
 C . M archand et al., JLAB proposal E 93-031;  
 D J. Tedeschiet al., JLAB proposals E 97-005 and E -98-109.